Ultrasonics 62 (2015) 292–298

Contents lists available at ScienceDirect

Ultrasonics

journal homepage: www.elsevier.com/locate/ultras

Inspection of additive-manufactured layered components

D. Cerniglia [a,*], M. Scafidi [a], A. Pantano [a], J. Rudlin [b]

[a] Dipartimento di Ingegneria Chimica, Gestionale, Informatica, Meccanica (DICGIM), Università di Palermo, viale delle Scienze, 90128 Palermo, Italy
[b] TWI Ltd., Granta Park, Abington, Cambridge CB21 6AL, UK

ARTICLE INFO

Article history:
Received 13 January 2015
Received in revised form 14 April 2015
Accepted 1 June 2015
Available online 7 June 2015

Keywords:
Laser powder deposition
Additive manufacturing
NDT inspection
Laser ultrasound
FEM

ABSTRACT

Laser powder deposition (LPD) is a rapid additive manufacturing process to produce, layer upon layer, 3D geometries or to repair high-value components. Currently there is no nondestructive technique that can guarantee absence of flaws in LPD products during manufacturing.

In this paper a laser ultrasonic technique for in-line inspection of LPD components is proposed. Reference samples were manufactured from Inconel and machined flaws were created to establish the sensitivity of the technique. Numerical models of laser-generated ultrasonic waves have been created to gain a deeper understanding of physics, to optimize the set-up and to verify the experimental measurements. Results obtained on two sets of reference samples are shown. A proof-of-concept prototype has been demonstrated on some specific deposition samples with induced flaws, that were confirmed by an ultra-high sensitivity X-ray technique. Experimental outcomes prove that typical micro-defects due to the layer-by-layer deposition process, such as near-surface and surface flaws in a single layer deposit, can be detected.

1. Introduction

Laser powder deposition (LPD) is an additive manufacturing process where layers are deposited, one after the other, to produce 3D geometries or to repair high-value components. A high-power laser beam is used to melt the powder material and, at the same time, a thin surface layer, so that they are bonded together [1–3]. The geometry of the component is built up, layer-by-layer, programming the path of the nozzle for the material deposition. Better accuracy and complexity can be achieved in products through additive manufacturing as compared to traditional manufacturing methods. Moreover, mechanical properties of additive manufacturing components approach and in some cases exceed the properties found in conventionally processed structures, as shown in [4]. The layer size is typically 0.5–2 mm wide and 0.3–0.5 mm deep. Interlayer and intralayer defects are often observed in laser deposited components as investigated in [5] using scanning electron microscopy and microcomputed tomography. The use of laser metal deposition to repair internal cracks in metallic components has been assessed in [6] although porosity is observed at the boundaries between the original part and the added material. The feasibility of laser metal deposition for repair applications with a procedure that leads to defect-free layers is shown in [7].

Additive manufacturing seems to be a potentially growing market in every manufacturing sector. In fact, in recent years, laser powder deposition has been established in several applications in a number of industries, including automotive, aerospace, military and medical. New and improved technologies, large application area and ease of development of custom products are the major drivers that can push the additive manufacturing market. However, a few factors restraining the growth of this market are material characterization during development, process control and quality control. In-line inspection has important implications for those sectors where validation of components, made using additive manufacturing techniques, has until now been difficult to achieve. Conventional nondestructive testing (NDT) techniques cannot cope with the complicated geometries and small sizes typically produced by additive manufacturing. Currently, the quality of LPD components is assessed by destructive testing or by X-ray computed tomography (CT) after the part is finished, which means that a sample may be rejected after all the manufacturing is completed. Moreover, the inspection should be carried out through many different slice images and X-ray CT may not have enough resolution for large parts.

For critical requirements of quality even in parts with complex forms, the desired solution is a nondestructive technique that allows the inline inspection and the detection of flaws as the layers are deposited, so that the process can be controlled and corrected. Some NDT methods have been investigated. The use of an

* Corresponding author. Tel.: +39 091 23897258.
E-mail address: donatella.cerniglia@unipa.it (D. Cerniglia).

http://dx.doi.org/10.1016/j.ultras.2015.06.001
0041-624X/

ultrasonic squirter probe with a standard industrial robot to inspect a 3D metal deposition structure is demonstrated in [8]. Laser-generated surface waves have been used in [9] to interrogate LPD parts, in both stainless steel and titanium, with pores that are simulated using blind holes. The potential of an all-optical scanning acoustic microscope instrument for online inspection of additive manufacturing products is shown in [10].

The laser ultrasonic technique was identified as a method that might be deployed for the inspection of LPD parts to detect near-surface and surface defects. The use of a laser transmitter and receiver and the interaction of the incident ultrasonic wave with sub-surface and surface defects have been widely investigated for many different applications, as demonstrated in [11–16].

The aim of this work is to prove the laser ultrasonic technique is a practicable solution for the inspection of LPD parts during manufacturing. A proof-of-concept prototype has been assembled and tested on different sets of reference samples and deposition samples with induced flaws. The performance of the inspection system is finally shown and discussed in the last part of the work.

2. Laser ultrasonic technique: experimental and numerical procedure

2.1. Experimental set-up

The laser ultrasonic system consists of an infrared Nd:YAG pulsed laser, used as source of acoustic waves, and a laser receiver, which combines a continuous-wave laser and an interferometric unit, to record the surface displacement. The two lasers have been assembled to create a laser system prototype. Wideband ultrasonic waves are generated with nanosecond laser pulses in the thermoelastic regime. The laser receiver produces a time-varying analog signal that is proportional to the instantaneous nanometric surface displacement. The output signals from the laser receiver are digitized at 8 bits by an analog-to-digital board converter, triggered by the pulsed laser, and transferred to a workstation for further signal processing and display. Fig. 1(a) shows the typical displacement of the surface wave (A-scan); its Fourier transform is shown in Fig. 1(b). The scanning procedure consists of acquiring a set of A-scans on the surface of the sample, following a line along the deposited layer. The two lasers beams are focused on two points of the line at a distance of 1.0 mm. The linear translation of the inspection system is possible by means of the LPD robot on which the system is mounted. The evaluation of the samples is done by acquiring the ultrasonic signals and the relative coordinates along the line, during scans at 0.1 mm steps. The data acquired on a line is processed through an algorithm to produce a B-scan image. For the complete inspection of the layer, more lines at an opportune distance are inspected producing more B-scans. The surface wave is monitored for sub-surface and surface defects, while reflection of bulk waves indicate inner discontinuities.

The laser system prototype was mounted on an attachment plate, bolted to the end plate of the LPD robot (Fig. 2). In this way, the inspection system needs only a translation from the robot deposition path, and then follows then the same path for the inspection.

The system should be able to determine the presence of a flaw in the component for a go/no-go selection of it. As described later, different sets of defective samples have been manufactured to determine the limits, in terms of size and depth, of the detectable flaws.

2.2. Samples

Reference samples, manufactured by TWI Ltd., have been used to establish the settings and to define a procedure for the inspection. Machined flaws were created in standard geometries to establish the sensitivity to defect detection. Laser machining and micro-Electric Discharge Machining (EDM) drilling were used to create holes in the Inconel samples, with different diameters (ϕ) and depths (d) below the surface. Two geometries of test samples are shown here: the first set (Type A) is an Inconel sheet with holes at different distances from the edge (Fig. 3(a)), the second (Type B) has a raised portion, representing the first layer above the substrate, where holes were drilled (Fig. 3(b)). After manufacturing, dimensions and depths of the holes were measured by high resolution microscopy. A summary of flaw sizes and depths in Type A and B samples is reported in Fig. 9, in the Results section.

Another set of samples was made with an Inconel substrate and a single layer deposit. Flaws were induced in each sample using different powder feed rates, laser power and speed of movement. Fig. 4 shows a typical flaw in a sectioned sample. Some samples had some substrate removed to determine the effect of the surface roughness on the technique.

2.3. Numerical analysis

Numerical models of laser-generated ultrasonic waves have been created to gain a deeper understanding of physics, to optimize the set-up and to verify the experimental measurements. Previous works [17–19] demonstrate that an explicit dynamic analysis together with the use of diagonal element mass matrices is computationally very efficient for the analysis of models with relatively short dynamic response times, as is the case for wave propagation with frequencies in the MHz range in relatively large

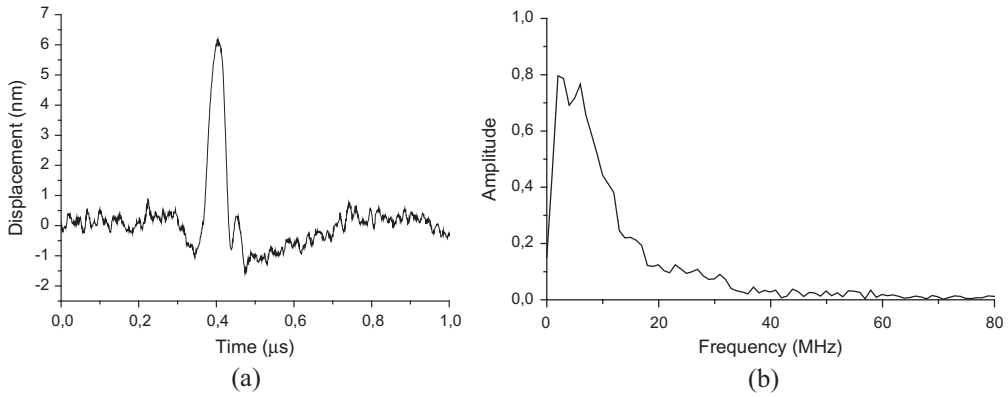

Fig. 1. Typical displacement of the surface wave (a) and its frequency content (b).

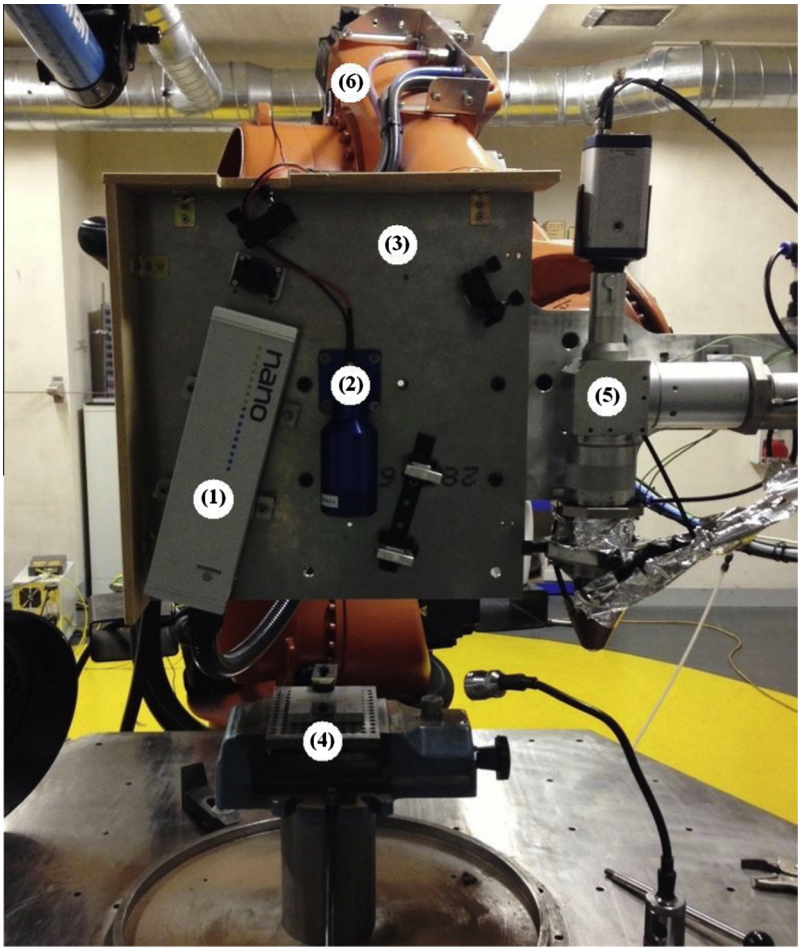

Fig. 2. The laser system mounted on the attachment plate and connected to the LPD robot: (1) laser transmitter, (2) laser receiver, (3) attachment plate, (4) LPD component, (5) LPD system, (6) robot.

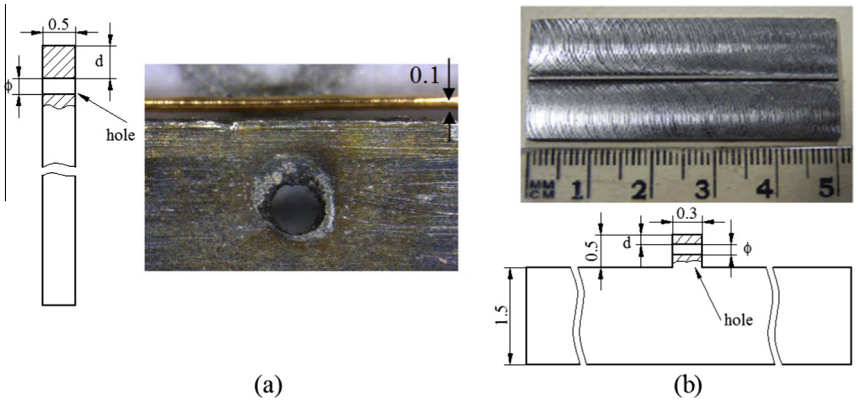

Fig. 3. (a) Section of Type A reference sample with hole, having diameter ϕ and depth d, made by laser drilling and high resolution microscopy image of the hole, showing the 0.1 mm copper wire as measuring scale; (b) section of Type B reference sample with hole, having diameter ϕ and depth d, made by EDM microdrilling. All dimensions are in mm.

bodies. The same method was implemented here. The following lines summarize the numerical technique.

A coupled thermal-stress analysis is required for modeling laser-generated ultrasound. The mechanical response is based on an explicit central-difference integration rule. The equations of heat transfer are integrated by an explicit forward-difference time integration rule. The explicit integration rule for the mechanical solution is combined with the use of diagonal element mass matrices, strongly improving the computational efficiency of the explicit procedure.

The laser source was simulated with a heat flux entering the surface of the model in the region hit by the laser beam. The value of laser power density that can be applied to the Inconel within the limit of the thermoelastic regime of generation was calculated to

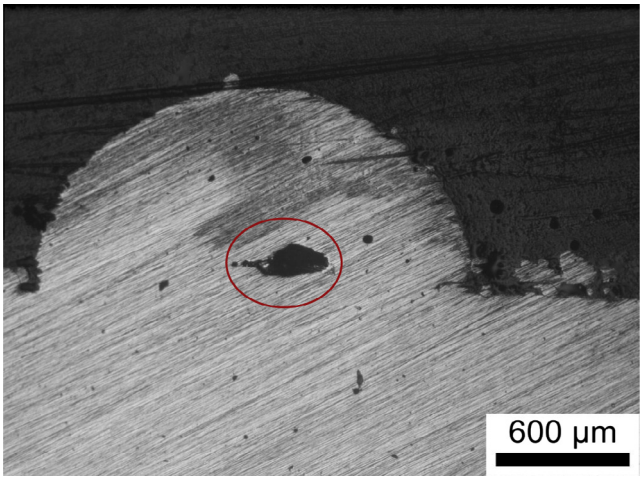

Fig. 4. Flaw induced in a Inconel deposit.

ensure the ablative regime of generation is not reached. The maximum absorbed laser flux density for the thermoelastic source according to [20] is:

$$I_0^{\max} = T_f \frac{\sqrt{\pi}K}{2\sqrt{kt_0}} = 12.4\ \mathrm{MW/cm^2} \quad (1)$$

where $T_f = 1354\ ^\circ\mathrm{C}$ is the melting temperature, $k = 14.9\ \mathrm{W/m\ ^\circ C}$ is the thermal conductivity, $k = 3.9 \cdot 10^{-6}\ \mathrm{m^2/s}$ is the thermal diffusivity and $t_0 = 5$ ns is the pulse duration. If this value of surface heat flux is used, the simulated displacements will be comparable with the real ones.

In order to obtain with the numerical analysis the signals acquired in the experimental part of this work, Rayleigh wave components up to 30 MHz should be detected. Under these circumstances the shortest wavelength to be analyzed is $\lambda_{\min} = c_R/f = 96$ μm where c_R, the Rayleigh wave velocity, is 2.88 mm/μs.

In explicit dynamics procedures, temporal and spatial resolution of the FE simulations are of crucial importance for the stability and the accuracy of the solution. The stability and accuracy of the solution in explicit dynamic procedures requires minimum temporal and spatial resolution of the FE simulations [21–25]. An accurate spatial resolution of the waves is guaranteed when the maximum size of the finite elements, l_e, is 1/10 of the shortest wavelength, $\lambda_{\min}$, to be analyzed: $l_e = \lambda_{\min}/10 = 9.6$ μm. An estimate of the limit of stability of the numerical method is often written as the smallest transit time of the wave through any of the elements in the mesh: $\Delta t = l_{\min}/c$ where $l_{\min}$ is the smallest element dimension in the mesh and c is the wave velocity. The temporal resolution of the explicit dynamic procedures modeling laser generated ultrasonic waves must be very small in order to correctly resolve their high frequencies components. Accurate solutions can be obtained if $\Delta t = 1/(20 \cdot f_{\max})$ where $f_{\max}$ is the highest frequency of interest. A realistic simulation of ultrasound propagation with frequencies reaching 30 MHz, requires the time increment Δt to be of the order of 10^{-9} s.

For the NDT set-up, two three-dimensional simulations were developed: the first to obtain the displacement pattern in the model without any defect, the second to collect the displacement when a hole is created in the model. All the material properties, boundary and load conditions replicated the conditions of the experiments. In defining the meshes of the two different numerical models, the one without any defect and the one with a hole, it is important to use the same mesh in the region outside of where the hole is located, otherwise it can adversely affect accuracy in a direct comparison between the two models.

Fig. 5 shows the detail of the meshed model without and with the hole. Both models were meshed by means of small tetrahedral elements with typical element edge lengths of 8.0 μm.

3. Results and discussion

3.1. Experimental results on reference samples

The inspection of each reference sample consisted of the A-scan signal collection along the simulated single layer deposit. Once the ultrasonic signals are acquired, the B-scan image is built by showing the magnitude of the normal displacement in a color map. The blue color correspond to the lower (negative) displacement, the red color to the maximum (positive) displacement. This method of displaying the signals was selected as the B-scan image emphasizes the presence of the wave perturbations due to the defect.

Some examples of the experimental displacement map built with the Type A and Type B reference samples are shown respectively in Figs. 6 and 7. Each B-scan image consists of 120 A-scan signals. The straight line in the map at about 0.4 μs represents the surface wave. Its disruption is the main mechanism by which surface and sub-surface flaws are detected; its sensitivity decreases significantly for flaws 100 μm below the surface, whatever the size. Additional indications come from the reflected waves due to the interaction of the bulk wave with the defect. This can be seen, in the zone with the hole, starting after the time of arrival of the longitudinal wave (i.e. 0.18 μs). Fig. 8 shows the numerical B-scan obtained by means of the 3D model reproducing the Type A reference sample, with hole size $\phi = 400$ μm and depth $d = 550$ μm. The numerical simulations compute displacements normal to the surface of the specimen. Times Of Flight (TOF) of the waves coincide with those of the corresponding experimental map shown in Fig. 6(c). The patterns of the curved wavefronts show a good match. The use of the finite element modeling approach appears to be an effective way of gaining a deeper understanding of ultrasonic wave propagation and ultimately of optimizing the set-up.

A summary of the capabilities of the technique for flaw detection in the reference samples is shown in Fig. 9. The results are based on the samples and procedures used in the experiments. The laser

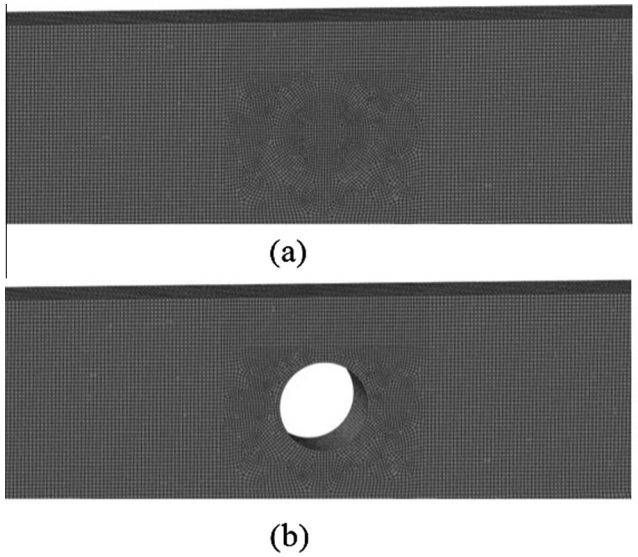

Fig. 5. Detail of the FE model without (a) and with the hole (b).

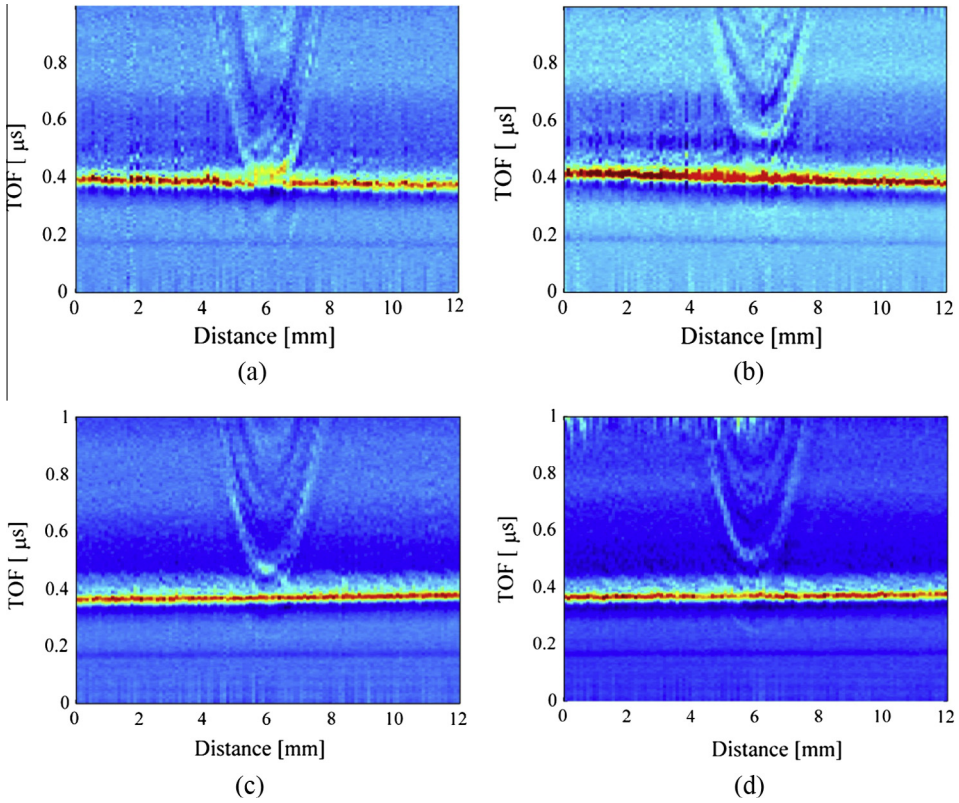

Fig. 6. Experimental B-scan of the Type A reference samples with hole size ϕ and depth d: ϕ = 500 μm, d = 300 μm (a), ϕ = 500 μm, d = 800 μm (b), ϕ = 400 μm, d = 550 μm (c) and ϕ = 400 μm, d = 700 μm (d).

ultrasonic technique is limited by the flaw sizes that can be detected. Flaws smaller than 100 μm were not detected unless they were surface breaking. Larger flaws can be easily detected if their depth is less than 300 μm. Deeper flaws up to 800 μm can be seen only if their size is such as to produce highly reflected waves.

3.2. Experimental results on induced flaw samples

The prototype has been demonstrated on a selection of deposition samples with induced flaws, similar to that shown in Fig. 4. Each sample was inspected with several unidirectional scans, at 0.2 mm distance across the deposit. Two example of B-scans are shown in Fig. 10. The indication of flaw is given in two consecutive scans for both samples; accordingly the width of the defects is less than 0.6 mm.

The presence of the flaws was confirmed by an ultra-high sensitivity X-ray technique inspection. The two indications have been measured in the film image planes and the relevant defect depths have been calculated by tilted exposures technique. Fig. 11 shows the indication images for the deposition samples with induced flaw. The defect size for Sample 05E5 (Fig. 11(a)) in the film image is 0.5 mm × 0.5 mm, while the depth is 0.7 mm and the calculated extension in thickness is 0.5 mm. The defect size for the Sample 05E7 (Fig. 11(b)) in the film image is 0.4 mm × 0.5 mm, where the depth is 0.4 mm and the calculated extension in thickness is 0.5 mm.

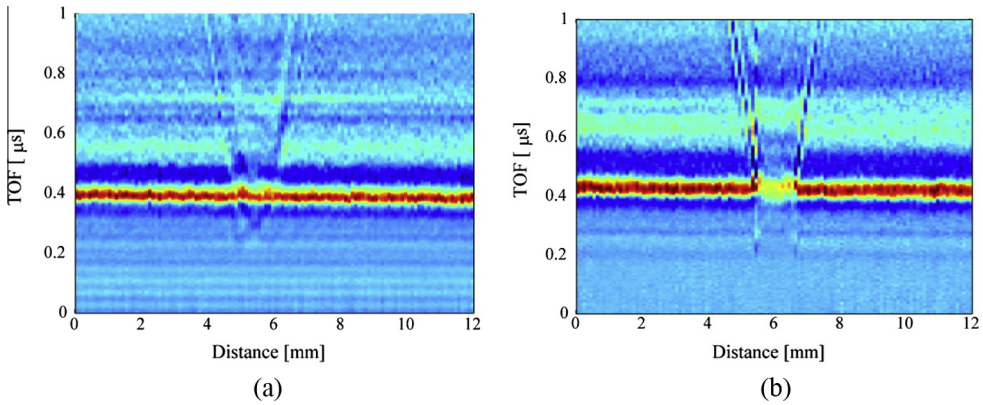

Fig. 7. Experimental B-scan of the Type B reference samples with hole size ϕ and depth d: ϕ = 154 μm, d = 135 μm (a) and ϕ = 150 μm, d = 13 μm (b).

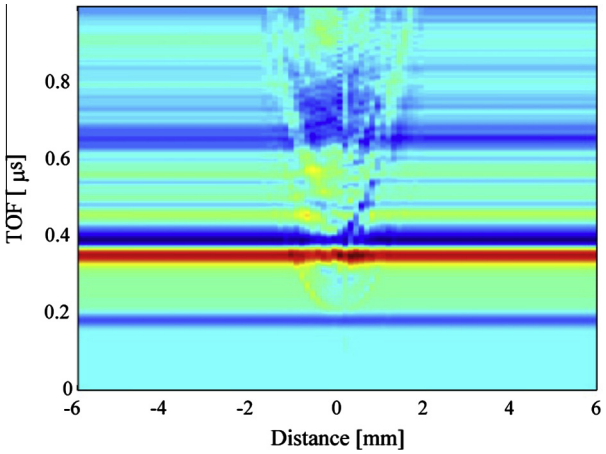

Fig. 8. Numerical B-scan obtained by means of the numerical approach in the 3D model reproducing the Type A reference sample, with hole size $\phi = 400$ µm and depth d = 550 µm.

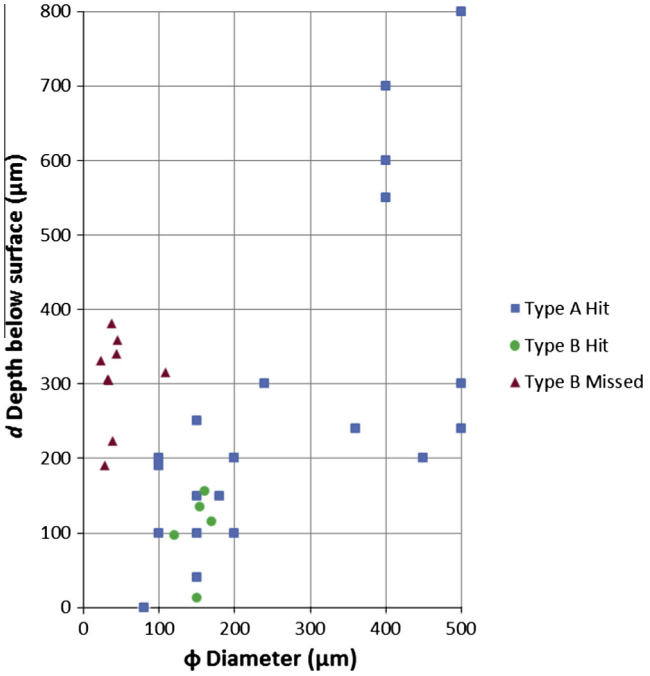

Fig. 9. Summary of flaw detection in the reference samples inspected by the laser ultrasonic technique.

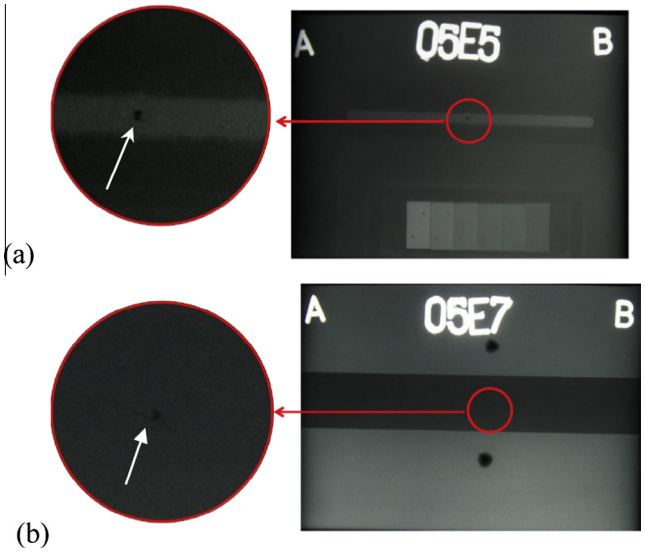

Fig. 11. Induced flaw in the deposition Samples 05E5 (a) and 05E7 (b), detected by ultra-high sensitivity X-ray technique.

The indications coming from these samples show that near-surface flaws in an Inconel deposit can be detected in the same way as in the reference samples.

4. Conclusion

Components manufactured with the rigorous process based on laser powder deposition require an equally rigorous inspection technique and one that operates over a small area. Additive manufacturing can create complicated geometries with small sizes and that is a big challenge for non-destructive testing methods. Currently, the quality of LPD components is assessed by destructive testing or by X-ray computed tomography after manufacturing is completed. The effectiveness of the laser ultrasonic technique to detect defects in LPD components has been proven to potentially inspect for flaws during manufacturing. Reference samples representing LPD parts and actual deposited samples have been manufactured and provided by TWI. The ultrasonic laser system was proven to be efficient for detecting micro-defects in the Inconel reference samples down to around 0.1 mm diameter, near the surface, and larger flaws up to 0.8 mm deep while no false positive indications were given for the flawless samples. A proof-of-concept prototype has been demonstrated on specific deposition samples with induced flaws, without any false positives.

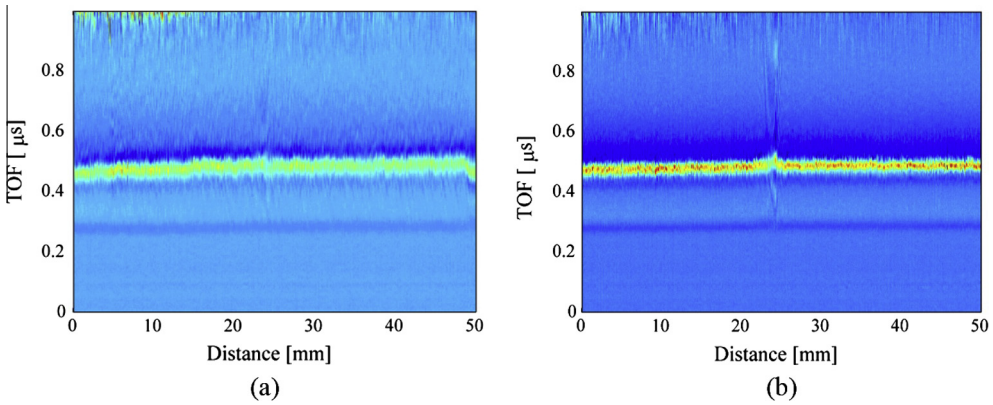

Fig. 10. B-scans of deposition Samples 05E5 (a) and 05E7 (b) on a 50 mm length with the indication of flaw.

The laser prototype can be incorporated into the LPD unit on a standard industrial robot, thus showing a high potential for an automated inspection system. The inspection can be performed immediately after the solidification of each layer.

Although the system has shown considerable potential, it will be necessary to carry out further developments to enable it to be used in a manufacturing process, with automated data processing and analysis. From other methods tested [26] this appears to be one of the most sensitive. The technique should also be easily adaptable to other metals and to other materials in which ultrasonic waves can be generated and detected by lasers. However, there are some limitations such as the effect of the surface. Moreover, the typical flaws that occur in manufacturing in different materials and alloy need to be known to optimize the procedure for specific manufacturing processes.

The cost of the equipment hardware and software is quite high, mostly because of the cost of the laser receiver, but if supplied with a laser deposition system including a robot, this will only represent a small part of the total cost.

Acknowledgments

The research leading to these results has received funding from the European Union FP7/2007-2013 Programme under Grant agreement 283833. Thanks are due to the SMEs in the project for permission to publish.

The authors would like to thank Roger Fairclough of TWI Sheffield for the preparation of the samples and Phil McNutt for controlling the robot. Thanks are also due to Bytest Srl for the X-ray analysis.

References

[1] I. Gibson, D.W. Rosen, B. Stucker, Additive Manufacturing Technologies: Rapid Prototyping to Direct Digital Manufacturing, Springer, US, 2010.
[2] I. Yadroitsev, A. Gusarov, I. Yadroitsava, I. Smurov, Single track formation in selective laser melting of metal powders, J. Mater. Process. Technol. 210 (2010) 1624–1631.
[3] G. Bi, A. Gasser, K. Wissenbach, A. Drenker, R. Poprawe, Characterization of the process control for the direct laser metallic powder deposition, Surf. Coat. Technol. 201 (6) (2006) 2676–2683.
[4] G.K. Lewis, E. Schlienger, Practical considerations and capabilities for laser assisted direct metal deposition, Mater. Des. 21 (2000) 417–423.
[5] M.N. Ahsan, R. Bradley, A.J. Pinkerton, Microcomputed tomography analysis of intralayer porosity generation in laser direct metal deposition and its causes, J. Laser Appl. 23 (2) (2011).
[6] A.J. Pinkerton, W. Wang, L. Li, Component repair using laser direct metal deposition, Proc. IMech Part B – J. Eng. Manuf. 222 (2008) 827–836.
[7] B. Graf, A. Gumenyuk, M. Rethmeier, Laser metal deposition as repair technology for stainless steel and titanium alloys, Phys. Proc. 39 (2012) 376–381.
[8] P. Nilsson, A. Appelgren, P. Henrikson, A. Runnemalm, Automatic ultrasonic testing for metal deposition, in: Proceedings of 18th World Conference on Nondestructive Testing, Durban, South Africa, 2012.
[9] J. Nemeth, M. Klien, J.W. Sears, Development of laser ultrasonics for defect detection during laser powder deposition, in: Proceedings of TMS Annual Meeting & Exhibition, San Francisco, CA, 2005.
[10] D. Clark, S.D. Sharples, D.C. Wright, Development of online inspection for additive manufacturing products, Insight 53 (11) (2011) 610–614.
[11] A.K. Kromine, P.A. Fomitchov, S. Krishnaswamy, J.D. Achenbach, Laser ultrasonic detection of surface breaking discontinuities: scanning laser source technique, Mater. Eval. 58 (2) (2000) 173–177.
[12] M. Arone, D. Cerniglia, V. Nigrelli, Defect characterization in Al welded joints by non-contact Lamb wave technique, J. Mater. Process. Technol. 176 (2006) 95–101.
[13] R.S. Edwards, B. Dutton, A.R. Clough, M.H. Rosli, Scanning Laser source and scanning laser detection techniques for different surface crack geometries, in: Review of Progress in Quantitative Nondestructive Evaluation, Proceedings of AIP Conference, Burlington, VT, 2011, pp. 251–258.
[14] Y. An, B. Park, H. Sohn, Complete noncontact laser ultrasonic imaging for automated crack visualization in a plate, Smart Mater. Struct. 22 (2013) 025022.
[15] F. Lanza di Scalea, R.E. Green Jr., High-sensitivity laser-based ultrasonic C-scan system for materials inspection, Exp. Mech. 39 (4) (1999) 329–334.
[16] I. Pelivanov, T. Buma, J. Xia, C. Wei, M. O'Donnel, A New fiber-optic non-contact compact laser-ultrasound scanner for fast non-destructive testing and evaluation of aircraft composites, J. Appl. Phys. 115 (2014) 113105.
[17] T. Ingrassia, V. Nigrelli, R. Buttitta, A comparison of simplex and simulated annealing for optimization of a new rear underrun protective device, Eng. Comput. 29 (2013) 345–358.
[18] A. Pantano, D. Cerniglia, Simulation of laser-generated ultrasonic wave propagation in solid media and air with application to NDE, Appl. Phys. A, Mater. Sci. Process. 98 (2010) 327–336.
[19] C. Mineo, D. Cerniglia, A. Pantano, Numerical study for a new methodology of flaws detection in train axles, Ultrasonics 54 (3) (2014) 841–849.
[20] C.B. Scruby, L.E. Drain, Laser Ultrasonics: Techniques and Applications, Adam Hilger, Bristol, 1990. pp. 228–235.
[21] F. Moser, L.J. Jacobs, J. Qu, Modelling elastic wave propagation in waveguides with the finite element method, NDT&E Int. 32 (1999) 225–234.
[22] B. Xu, Z. Shen, J. Wang, X. Ni, J. Guan, J. Lu, Thermoelastic finite element modelling of laser generation ultrasound, J. Appl. Phys. 99 (2006). 33508–1 to 7.
[23] W. Hassan, W. Veronesi, Finite element analysis of Rayleigh wave interaction with finite-size surface-breaking cracks, Ultrasonics 41 (2003) 41–52.
[24] A. Zerwer, M.A. Polak, J.C. Santamarina, Rayleigh wave propagation for the detection of near surface discontinuities: finite element study, J. Nondestruct. Eval. 22 (2003) 39–52.
[25] H. Jeong, M.C. Park, Finite-element analysis of laser-generated ultrasounds for wave propagation and interaction with surface-breaking cracks, Res. Nondestruct. Eval. 16 (2005) 1–14.
[26] J. Rudlin, D. Cerniglia, M. Scafidi, C. Schneider, Inspection of laser powder deposited layers, in: Proceedings of 11th European Conference on NDT, Prague, Czech Republic, 2014.